Computational Modelling of Concrete and Concrete Structures – Meschke, Pichler & Rots (Eds)

How gap tests of ductile and quasibrittle fracture limit applicability of phase-field, XFEM, cohesive, nonlocal and crack-band models?

Z.P. Bažant
Northwestern University, USA

A.A. Dönmez
Northwestern University, USA
Istanbul Technical University, Turkey

H.T. Nguyen
Northwestern University, USA

ABSTRACT: The recently developed gap test exploits the size effect method to determine the effect of crack-parallel compression σ_{xx} on the material fracture energy, G_f, as well as the characteristic size c_f of the fracture process zone (FPZ). The previous gap tests demonstrated that the G_f of concrete can get doubled or reduced to almost zero according to the T-stress (crack-parallel stress) level. A subsequent study of aluminum fracture (Nguyen, Dönmez and Bažant, 2021) concluded that a similar effect exists in ductile fracture of polycrystalline plastic-hardening metals. This paper strengthens this conclusion by presenting and interpreting further gap tests of aluminum. Together with the results of the recent gap tests of crack-parallel stress effect in quasibrittle materials, the experimental evidence shows that the linear elastic fracture mechanics (LEFM), its computational versions XFEM and Phase-Field, and the cohesive crack models are inapplicable in the presence of significant crack-parallel stress—not only for concrete and other quasibrittle materials but also for plastic-hardening polycrystalline metals. On the other hand, the applicability of the crack band model with a realistic tensorial damage law is not limited.

1 INTRODUCTION

A complicating feature of the plastic-hardening metals is that large hardening yielding zone surrounding the fracture front in which the material undergoes softening damage was studied analytically, considering only σ_{xx} in the propagation direction, although the out-of-plane normal and shear components, σ_{zz} and σ_{xz}, of the crack-parallel stress are also expected to play a significant role, as already confirmed for σ_{zz} in concrete (H. Nguyen *et al.* 2020) and shown here for aluminum. Asymptotic matching was used to formulate the general scaling laws of plastic-hardening polycrystalline metals. These laws were related to the material fracture energy G_f as well as the effective radius of the yielding zone, r_p.

In this study, an extension of these gap tests and their theoretical consequences is presented. The changes in the energetic size effect are studied experimentally over a much broader range of crack-parallel compressive stress σ_{xx} and a broader size range. Then the size effect method (Bažant et al. 1991; Bažant & Planas 1997; Nguyen et al. 2021) is used to deduce from these changes the effect of σ_{xx} on the material fracture energy, G_f, and on the effective radius r_p of the yielding zone (YZ) of aluminum. The effect of σ_{xx} on the scaling asymptotes of the small-scale-yielding is also clarified. However, because the range of specimen sizes in this study is much greater than the inhomogeneity size (which is the size of a polycrystalline grain, about 2 to 50 micrometers), the change in the size of the YZ and the fracture process zone (FPZ) can only be distinguished using numerical models.

2 ASYMPTOTIC SCALING REGIMES

The analytical solution of the role of the large yielding zone surrounding the fracture front was studied in recent works (Bažant et al. 2022; Nguyen et al. 2021). A brief review of the hardening plasticity and yielding zone effect on fracture is given here.

The polycrystalline metals have very small FPZ, of micrometer-scale, compared to the millimeter-scale plastic hardening part or the yielding zone. This introduces one more transitional range in the original SEL of Type 2. That additional transition is shown in Figure 1. As shown in Figure 1, three size effects can be considered in the Al alloys and other polycrystalline metals; the transition from the FPZ to large-scale yielding, the transition from the large-scale to small-scale yielding, or LEFM (linear elastic fracture mechanics—the

DOI 10.1201/9781003316404-48

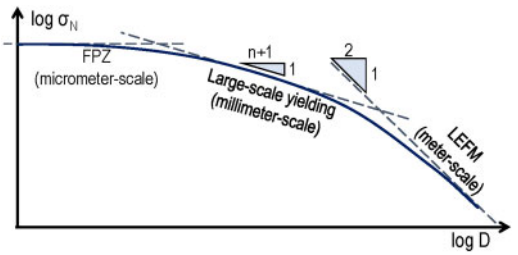

Figure 1. Description of the three transitional zones and the asymptotes in fracture of plastic-hardening polycrystalline metals.

large-scale asymptote for LEFM), and finally the overall transition from the FPZ (micrometer-scale) to small-scale yielding (LEFM). The second transition involves a deviation from the original size effect law. The third transition corresponds to the SEL and is probably the most important one among the three transitional regimes.

3 REVIEW OF STRESS-STRAIN RELATION OF PLASTIC-HARDENNING METALS

The plastic hardening response of metals can be defined by the Ramberg-Osgood model for the uniaxial stress-strain law (Fig. 2) (Ramberg & Osgood 1943).

$$\frac{\varepsilon}{\varepsilon_y} = \frac{\sigma}{\sigma_y} + \alpha_p \left(\frac{\sigma}{\sigma_y}\right)^n \tag{1}$$

where ε_y = initial yield strain, σ_y = initial yield strength; α_p = empirical parameter (usually denoted as α, although α is the standard notation for a dimensionless crack length); and n = plastic hardening exponent, typically 3 to 20. For analysis, it is helpful that the n, the hardening exponent, is so high that the plastic strain dominates and the elastic strain can be ignored. This assumption was the basis of the

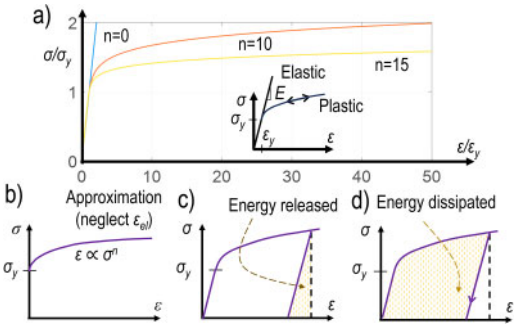

Figure 2. (a) Stress-strain behavior of plastic-hardening metals and response curves for various n(hardening exponent). (b) Approximation when elastic strain is ignored; Elastoplastic constitutive law with various n; (c,d) The partition of strain energy into released and dissipated.

classical Hutchinson-Rice-Rosengren (HRR) theory (Hutchinson 1968; Rice & Rosengren, 1968).

The advantage of the power law in Eq. (1) is that the stress-strain law becomes self-similar for the strain or stress magnitude. Together with the divided form of the power-law singularity, broadly presented as required (Nguyen et al. 2021), the deformation-field at the near-tip asymptote becomes self-similar to radial affine transformations, which makes it feasible for an analytical solution. The uniaxial stress-strain relation is therefore stated as (Hutchinson 1968; Rice & Rosengren 1968):

$$\frac{\varepsilon}{\varepsilon_y} - \alpha_p \left(\frac{\sigma}{\sigma_y}\right)^n \tag{2}$$

$$e_{ij} - \frac{3\alpha_p \varepsilon_y}{2\sigma_y} \left(\frac{\sigma_{ef}}{\sigma_y}\right)^{n-1} \tag{3}$$

$$\sigma_{ef} = \sqrt{\frac{3}{2} s_{kl} s_{kl}} \tag{4}$$

The uniaxial yield stress, σ_y, and the uniaxial yield strain, ε_y, in Eq. (2-4) are the limiting parameters for the effective (or equivalent) yield stress. These parameters point out the distinction of the power-law strain from the previous (largely elastic) regime. The σ_y in Eq. (4) is the scalar effective stress.

Hutchinson and Paris in (Hutchinson & Paris 1979) showed that the deformation theory of plasticity is very accurate in this problem, although its use is a simplifying assumption in the HRR theory and the J-integral.

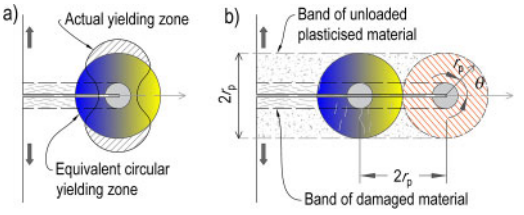

Figure 3. (a) Actual and equivalent (equal area or volume) yielding zones; (b) displacement of the equivalent yielding zone with the crack growth.

Figure 3 illustrates the yielding zone and the approximately equivalent crack growth model. In Figure 3, the (r, θ) are the polar coordinates centered at the tip of the crack. The angle θ is measured from the crack extension line and r_p is the effective size of the hardening part (or the yielding zone, YZ).

4 SIZE EFFECT DUE TO ENERGY RELEASE

The energy balance equation can be constructed by using the physical similarities of the ductile and quasibrittle failures with respect to the transitional regimes, as used in (Nguyen et al. 2021). The energy

release rates, G_s and G_p arise from two different locations in the structure. The G_s is the rate of energy release from the elastic zone in the structure (or from the undamaged volume of the structure). This energy release is approximately proportional to the characteristic size, D. Second, G_b is the energy release rate from the elastic material traversed by the front of the crack band. It does not depend on D. Note that there is no plastic yielding zone in quasibrittle materials, unlike the plastic hardening metals where the large yielding zone causes a transition between the FPZ and the elastic zone of the structure.

The yielding zone, which is typically of millimeter scale, plays three roles in the failure mechanism. First, it transfers the energy-flux to the FPZ via the yielding zone. The energy is conserved in this transfer. Second, the yielding zone dissipates energy in its wake, with the rate of G_p, as the plastically strained material undergoes unloading. Third, the unloading of the plasticized material in the wake of the advancing yielding zone releases its strain energy, with the rate of G_b. The G_b is defined as the strain energy, $(\gamma_c \sigma_N)^2/2\mathrm{E}'$, that was contained in the band of width $2r_p$ prior to the arrival of the yielding zone. Therefore, the energy balance during fracture can be written as:

$$G_s + G_b = G_f + G_p \tag{5}$$

We may use a fixed characteristic length scale for G_b, similar to c_f, defined by the yielding zone width $(2r_p)$: $G_b = (\sigma_N^2/E')2r_p$. For G_s we can use the same expression as in quasibrittle materials. Inserting in (5) the energy release rate expressions, we obtain the condition of energy conservation:

$$\frac{\sigma_N^2}{E'} D g_0 + \frac{\sigma_N^2}{E'} 2r_p = G_f + G_p \tag{6}$$

Solving for σ_N, we get the size effect law for fracture of plastic-hardening metals in small-scale yielding:

$$\sigma_N = \frac{\sigma_0}{\sqrt{1 + D/D_0}} \tag{7}$$

Eq. (7) has the same form as the SEL for quasibrittle failures. However, the definitions of its coefficients are not the same:

$$\sigma_0^2 = E' G_f / 2r_p + \sigma_p^2, D_0 = 2r_p / g_0 \tag{8}$$

$$\sigma_p^2 = \frac{1}{2} E' \sigma_y ?_y Q_p \tag{9}$$

The asymptotes of this law have the same slopes as SEL:

$$\sigma_N \underset{D\to 0}{\Rightarrow} \sigma_0 = \text{constant}, \sigma_N \underset{D\to 0}{\Rightarrow} D^{-1/2} \tag{10}$$

The underlying assumption is that r_p is about the same for all specimen sizes. The "triaxiality number" (Anderson 2017) is assumed to remain constant, too.

5 SIZE EFFECT METHOD FOR DUCTILE FRACTURE

The size effect on structural strength is the main consequence of fracture behavior, and the size effect method is the most straightforward and unambiguous procedure to identify the material fracture properties. Eq. (7) can be restated as linear regression:

$$Y = AX + C \text{where} X = D; \quad Y = 1/\sigma_N^2 \tag{11}$$

$$A = 1/\sigma_0^2 D_0, \quad C = 1/\sigma_0^2 \tag{12}$$

The fracture energy, G_f, and the effective width of the yielding zone, $2r_p$, can be obtained by fitting these equations with the test results. The required test data consist only of the peak loads (max. loads) of differently sized specimens with a sufficiently broad size range. After getting the dimensionless energy release rate g_0 (and E'), one can find the A and C values by a linear regression of the data in the plane (X, Y). Then one can get $\sigma_0 = 1/\sqrt{C}$ and $D_0 = C/A$ using these values from the regression analysis. Finally, the fracture parameters can be obtained as:

$$G_f = (C^{-\frac{1}{2}} - c_p) g_0 / E' g_0^2 A, \quad r_p = \frac{g_0}{2\sigma_0^2 A} \tag{13}$$

6 GAP TESTS OF ALUMINUM

In the standard fracture specimens, the stresses $\sigma_{xx}, \sigma_{zz}, \sigma_{xz}$ parallel to the crack plane (x, z) are zero or negligible. It has been implicitly assumed that the cracks are planes with zero thicknesses. If this assumption were correct, then no effect of $\sigma_{xx}, \sigma_{zz}, \sigma_{xz}$ on the crack propagation could be expected. Actually, the FPZ, located in front of the crack tip, has always a finite width, δ_y, measured normal to its plane. This is the fundamental characteristic of the blunt crack (Bažant & Cedolin 1991) and crack band (Bažant 1993; Bažant & Oh 1983) models, which revealed already in 1979 that, if δ_y is finite, the effect of $\sigma_{xx}, \sigma_{zz}, \sigma_{xz}$ must be important and the damage tensor inside the fracture process zone must play a role, and that the scalar stress-displacement law of the cohesive (or fictitious) crack model is inadequate. Some role of the crack-parallel compression in concrete has long ago been suspected by a few researchers (Bažant 1993; Bažant & Cedolin 1979; Bažant & Oh 1983; Tschegg et al. 1995), but a simple unambiguous test had been unavailable until the new gap test was developed, in 2020 (Bažant et al. 2022; H. Nguyen *et al.*, 2020; H. T. Nguyen *et al.*, 2020; Nguyen et al. 2021).

The gap tests conducted here involve notched beam specimens of aluminum, the 6061 series. The specimens are scaled geometrically in compliance with the $2D$ scaling laws, with a fixed width of 10 mm, as shown in Figure 4a, b. Their depths are 12, 24, 48 and, 96 mm. Figs. 4c, d show the results of standard three-point bend tests (no crack-parallel compression). The

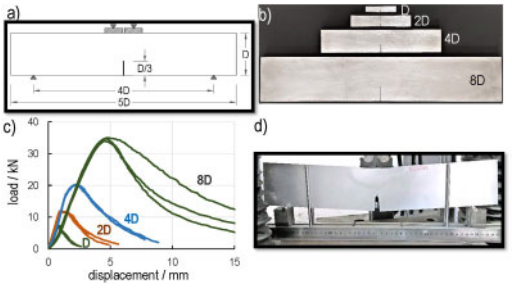

Figure 4. The geometrical properties of the specimens; (b) the scaled specimens of four sizes, with the fixed thickness; (c) Load vs. mid-span deflection curves; (d) the post-failure image showing the crack in the largest specimen.

deformed state of the largest specimen can be seen in Figure 4d.

The resulting size effect curves are shown in Figure 5. The data points in Figure 5a represent the measured peak values of nominal strength σ_N for scaled gap tests of 4 different sizes $D = 12, 24, 48, 96$ mm, and for three different levels of crack-parallel compression.

In Figure 5a, the crack-parallel stress, σ_{xx}, is presented relative to the yield strength (f_y) of the Al alloy, which is has been measured as 450MPa in the uniaxial compression tests. The three solid curves display the best-fit curves obtained by multivariate nonlinear regression analysis of the data points with the size effect law. The systematic pattern of the curves shows the scatter to be relatively small compared to the overall scatter of all data.

In Figure 5a, the LEFM size effect slope of $-1/2$ is still far from being achieved, even for the largest specimens. This means that a much larger size would be needed to reach the LEFM range (which is the small-scale yielding range). Furthermore, the position of the LEFM asymptote of $-1/2$ determines the fracture energy, G_f (which is equal to J_{cr} and represents a new way of measuring it). The LEFM is displayed as the dashed line for the case of the largest crack-parallel compression. A translation of the LEFM asymptote to the right implies an increase of G_f. These LEFM asymptotes for the three levels of crack-parallel compression (σ_{xx}) are shifted relative to each other (Fig. 5a), which means that the fracture energies of these three cases are different.

The estimates of G_{FPZ}, asapartof the ΔG_f, can be evaluated from the size effect curves and their corresponding fracture parameters. It is known that, for the same crack-parallel stress σ_{xx} (also called the T-stress), the size of the yielding zone in front of the crack tip does not change and stays approximately the same for every size, D. In other words, the dissipation of the energy from the wake of the yielding zone is size-independent for the same T-stress. Thus, the discrepancy in the size effect fits from the gap tests, must be explained by a change of the energy dissipation in the micrometer-scale fracture process zone of the polycrystalline metal.

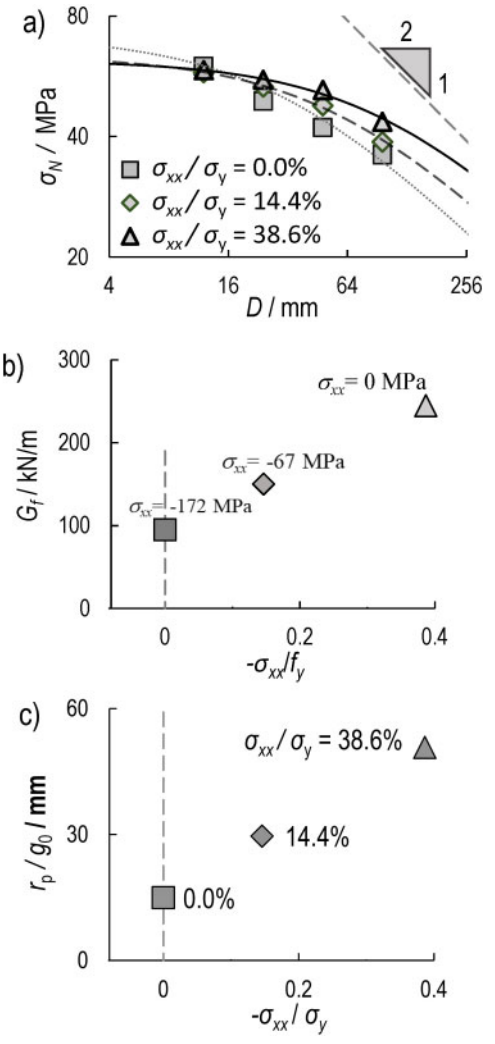

Figure 5. (a) Measured size effect data of aluminum for four different specimen sizes D and three different ratios of crack-parallel stress σ_{xx} to yield strength f_y, in logarithmic scales; Experimentally obtained data on the dependence of (b) fracture energy G_f and (c) half width of yielding zone r_p on the ratio of crack-parallel compressive stress σ_{xx} to yield strength f_y.

Consequently, the variation of the fracture energies (G_f) presented in Figure 5b results from a change of both the FPZ (at the micrometer scale) and the yielding zone. Nevertheless, this difference was around 10-30 mm, implying a much more marked contribution from the yielding zone. To differentiate the contributions from these two zones would require either micrometer-scale gap tests or numerical computational results with a realistic damage constitutive model for aluminum. The numerical models for capturing the effects of crack-parallel compression on the strength, size effect, and fracture parameters, require a tensorial damage constitutive law. The phase-field, XFEM, and cohesive crack model cannot capture such effects.

7 CONSEQUENCES FOR APPLICABILITY OF LEFM (WITH XFEM), PHASE-FIELD AND COHESIVE CRACK MODELS

Extension of the gap tests of aluminum to three different levels of the crack-parallel compressive stress σ_{xx} provides clear evidence of the effect of σ_{xx} on the size effect, which is found to be strong. Regression analysis of the gap tests of different sizes for the same σ_{xx} level yields unambiguous evidence of the σ_{xx} effect on the fracture energy G_f of aluminum. Increasing σ_{xx} from 0 to $0.4f_y$, causes G_f to approximately double and r_p to triple (see Fig. 5c). Although no tests were made at $|\sigma_{xx}| > 0.4f_y$, the extension of the curve of G_f versus σ_{xx} is expected not to tend to 0 at $\sigma_{xx} \to -f_y$ because, in contrast to concrete, aluminum yielding under compression in x-direction suffers no softening damages and yields at increasing strength in the y-direction. To reproduce the present experiments mathematically, a fracture process zone of correct finite width, described by a realistic tensorial damage constitutive model for aluminum, will be used in subsequent work. The finite element crack band model serves well for that.

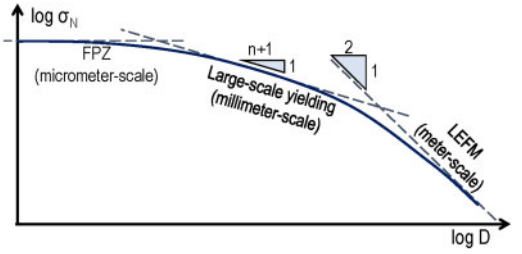

Figure 6. Path dependence of G_f as a function of σ_{xx} (if path dependence were absent, the terminal points encircled by ellipses would have to coincide).

It might be thought that the aforementioned models could be used if the fracture energy, G_f, were considered to be a function of σ_{xx}. However, this is not possible because the dependence of G_f on σ_{xx} is enormously path-dependent (H. Nguyen *et al.*, 2020; H. T. Nguyen *et al.*, 2020), as shown in Fig. 6. There is no way to shrink the FPZ to a line and thus obtain a line crack, except if the crack-parallel stresses are negligible, which is, however, a rare situation in practice.

8 CONCLUSIONS

As a result of the gap tests, the classical fracture mechanics dealing with line cracks is now seen to be severely limited. Nevertheless, this fundamental theory remains necessary for the understanding of brittle and quasibrittle structural failures, for underpinning blunt crack models, and for teaching the fracture behavior of structures.

ACKNOWLEDGMENT

Funding under NSF Grant CMMI-1439960 to Northwestern University is gratefully acknowledged. A.A.D also thanks for funding from Istanbul Technical University, BAP:42833. Conflict of interest: None.

REFERENCES

Anderson, T. (2017) *Fracture Mechanics: Fundamentals and Applications*. 4th edn. Boca Raton, London, New York: CRC Press.

Bažant, Z. P. (1993) 'Scaling Laws in Mechanics of Failure', *Journal of Engineering Mechanics*. American Society of Civil Engineers (ASCE), 119(9), pp. 1828–1844.

Bažant, Z. P. and Cedolin, L. (1979) 'Blunt Crack Band Propagation in Finite Element Analysis', *Journal of the Engineering Mechanics Division*. American Society of Civil Engineers, 105(2), pp. 297–315.

Bažant, Z. P. and Cedolin, L. (1991) *Stability of Structures: Elastic, Inelastic, Fracture and Damage Theories, 2010*. World Scientific Publishing Co. Pte. Lfd., ISBN-13.

Bažant, Z. P., Dönmez, A. A. and Nguyen, H. T. (2022) 'Précis of gap test results requiring reappraisal of line crack and phase-field models of fracture mechanics', *Engineering Structures*, 250, p. 113285.

Bažant, Z. P., Kazemi, M. T. and others (1991) 'Size effect on diagonal shear failure of beams without stirrups', *ACI Structural journal*, 88(3), pp. 268–276.

Bažant, Z. P. and Oh, B. H. (1983) 'Crack band theory for fracture of concrete', *Matériaux et construction*. Springer, 16(3), pp. 155–177.

Bažant, Z. P. and Planas, J. (1997) *Fracture and size effect in concrete and other quasibrittle materials*. Boca Raton, Boston, London: CRC press.

Hutchinson, J. W. (1968) 'Singular behaviour at the end of a tensile crack in a hardening material', *Journal of the Mechanics and Physics of Solids*, 16(1), pp. 13–31.

Hutchinson, J. W. and Paris, P. C. (1979) 'Stability Analysis of J-Controlled Crack Growth', *Elastic-Plastic Fracture*. ASTM International, p. 64.

Nguyen, H. *et al.* (2020) 'New perspective of fracture mechanics inspired by gap test with crack-parallel compression', *Proceedings of the National Academy of Sciences of the United States of America*. National Academy of Sciences, 117(25), pp. 14015–14020.

Nguyen, H. T. *et al.* (2020) 'Gap Test of Crack-Parallel Stress Effect on Quasibrittle Fracture and Its Consequences', *Journal of Applied Mechanics*, 87(7), p. 071012.

Nguyen, H. T., Dönmez, A. A. and Bažant, Z. P. (2021) 'Structural strength scaling law for fracture of plastic-hardening metals and testing of fracture properties', *Extreme Mechanics Letter*, 43, p. 101141.

Ramberg, W. and Osgood, W. R. (1943) *Description of stress-strain curves by three parameters*. Washington.

Rice, J. R. and Rosengren, G. F. G. (1968) 'Plane strain deformation near a crack tip in a power-law hardening material', *Journal of the Mechanics and Physics of Solids*. Pergamon, 16(1), pp. 1–12.

Tschegg, E. K., Elser, M. and Stanzl-Tschegg, S. E. (1995) 'Biaxial fracture tests on concrete — Development and experience', *Cement and Concrete Composites*. Elsevier, 17(1), pp. 57–75.